Antimicrobial peptide derived from insulin-like growth factor-binding protein 5 improves diabetic wound healing

Hainan Yue, MD[1,2], Pu Song, MD, PhD[3], Nutda Sutthammikorn, PhD[4], Yoshie Umehara, PhD[2], Juan Valentin Trujillo-Paez, PhD[2], Hai Le Thanh Nguyen, MD[1,2], Miho Takahashi, MD[1,2], Ge Peng, MD[1,2], Risa Ikutama, MD[1,2], Ko Okumura, MD, PhD[2], Hideoki Ogawa, MD, PhD[2], Shigaku Ikeda, MD, PhD[1,2], François Niyonsaba, MD, PhD[2,5]*

[1]Department of Dermatology and Allergology and [2]Atopy (Allergy) Research Center, Juntendo University Graduate School of Medicine, Tokyo, Japan. [3]Department of Dermatology, Xijing Hospital, Fourth Military Medical University, Xi'an, Shannxi, China. [4]Department of Microbiology, Faculty of Medicine, Chiang Mai University, Chiang Mai, Thailand. [5]Faculty of International Liberal Arts, Juntendo University, Tokyo, Japan.

***Correspondence:** François Niyonsaba. Juntendo University, 2-1-1 Hongo, Bunkyo-ku, Tokyo 113-8421, Japan. Email: francois@juntendo.ac.jp. Telephone number: +81-3-5802-1591; Fax number: +81-3-3813-5512.

Keywords: diabetic wound, keratinocyte, antimicrobial peptide, high glucose, angiogenesis

Abstract

Impaired keratinocyte functions are major factors that are responsible for delayed diabetic wound healing. In addition to its antimicrobial activity, the antimicrobial peptide derived from insulin-like growth factor-binding protein 5 (AMP-IBP5) activates mast cells and promotes keratinocyte and fibroblast proliferation and migration. However, its effects on diabetic wound healing remain unclear. Human keratinocytes were cultured in normal or high glucose milieus. The production of angiogenic growth factor and cell proliferation and migration were evaluated. Wounds in normal and streptozotocin-induced diabetic mice were monitored and histologically examined. We found that AMP-IBP5 rescued the high glucose-induced attenuation of proliferation and migration as well as the production of angiogenin and vascular endothelial growth factor in keratinocytes. AMP-IBP5-induced activity was mediated by the epidermal growth factor receptor, signal transducer and activator of transcription 1 and 3, and mitogen-activated protein kinase pathways, as indicated by the inhibitory effects of pathway-specific inhibitors. *In vivo*, AMP-IBP5 markedly accelerated wound healing, increased the expression of angiogenic factors and promoted vessel formation in both normal and diabetic mice. Overall, the finding that AMP-IBP5 accelerated diabetic wound healing by protecting against glucotoxicity and promoting angiogenesis suggests that AMP-IBP5 might be a potential therapeutic target for treating chronic diabetic wounds.

1 Introduction

Diabetes mellitus is a serious public health problem associated with long-term consequences that impacts the quality of life of individuals and their families. The prevalence of diabetes is increasing and is estimated to be 10.2% (578 million) by 2030 and 10.9% (700 million) by 2045.[1] The global prevalence of diabetic foot ulcers is as high as 6.3% due to the increasing worldwide prevalence of diabetes and the prolonged life expectancy of diabetic patients.[2] It has been reported that every 30 seconds, the lower limb or part of a lower limb is amputated in diabetic patients due to foot ulcers worldwide.[3] Although a wide range of treatment strategies, such as customized dressings, negative pressure wound therapy, hyperbaric oxygen treatment, debridement, topical growth factor application and stem-cell therapy, have been proposed for diabetic wound therapy, the etiological complexity of impaired wound healing in patients with diabetes often leads to unsatisfactory results, as there is a lack of holistic strategies to resolve this issue.[4-6] Therefore, there is a high unmet need for the development of novel therapeutic strategies for the treatment of diabetic wounds.

Impaired diabetic wound healing involves multiple factors, including hypoxia, epidermal cell dysfunction, impaired angiogenesis and neovascularization, infections, glucotoxicity, decreased host immune resistance, and neuropathy.[7-10] Keratinocytes play a crucial role in re-epithelialization and angiogenesis via migration, proliferation, and the secretion of cytokines and antimicrobial peptides (AMPs).[11,12] Several hypotheses suggest that hyperglycemia-

induced disturbances in keratinocyte functions, including the inhibition of migration and proliferation, impairment of angiogenesis, and downregulation of AMPs and cytokines, are important factors that contribute to poor diabetic wound healing.[7,13,14]

Antimicrobial peptide derived from insulin-like growth factor-binding protein 5 (AMP-IBP5) is a newly discovered AMP produced by the defined proteolytic processing of insulin-like growth factor-binding protein 5 (IGFBP5) via serine proteases such as prohormone convertases and carboxypeptidase.[15] Although AMPs were initially well known for their antimicrobial activities, increasing evidence suggests that these molecules, such as human β-defensin (hBD)-2, hBD-3 and cathelicidin LL-37, also exert multiple immunomodulatory effects, including the modulation of inflammation, promotion of cell proliferation and migration, induction of angiogenesis, and improvements in skin barrier function and wound healing.[8,16,17] LL-37 promotes keratinocyte migration through activation of the epidermal growth factor receptor (EGFR) and signal transducer and activator of transcription (STAT) pathways.[18] Furthermore, recent studies indicated that AMP-IBP5 induces the proliferation and migration of keratinocytes and fibroblasts, enhances the secretion of angiogenin (ANG) and vascular endothelial growth factor (VEGF), and promotes the activation of mast cells,[19-21] indicating that AMP-IBP5 might play an important role in the wound healing process.

Although AMP-IBP5 is thought to contribute to wound healing, its potential effects on diabetic wounds and the underlying mechanisms remain unexplored. We hypothesized that

AMP-IBP5 might counteract the negative effects of high glucose on keratinocytes and promote diabetic wound healing through the activation of EGFR/STAT and MAPK pathways as well as promote proliferation, migration and angiogenesis in keratinocytes.

2 Materials and methods

2.1 Reagents

AMP-IBP5 (AVYLPNCDRKGFYKRKQCKPSR-NH_2) was obtained from the Peptide Institute (Osaka, Japan). Rabbit anti-CD31 antibody was obtained from Abcam (Tokyo, Japan). IgG isotype control and antibodies against phosphorylated and unphosphorylated EGFR, STAT1, STAT3, ERK, JNK and p38 were purchased from Cell Signaling Technology (Beverly, MA). Goat anti-rabbit Alexa Fluor 594 was purchased from Invitrogen (Carlsbad, CA). Normal goat serum was obtained from Vector (Burlingame, CA). Mouse anti-Ki67 monoclonal antibody was obtained from Invitrogen. Streptozotocin was purchased from Sigma–Aldrich (St Louis, MO). AG1478 was obtained from Santa Cruz Biotechnology (Dallas, TX). Fludarabine and cryptotanshinone were purchased from Cayman Chemical (Ann Arbor, MI). U0126, SB203580 and JNK inhibitor II were obtained from Calbiochem (La Jolla, CA). Enzyme-linked immunosorbent assay (ELISA) kits were obtained from R&D Systems (Minneapolis, MN). Mitomycin C and crystal violet were obtained from the Fujifilm Wako Pure Chemical Corporation (Tokyo, Japan).

2.2 Mouse model and treatment

Male C57BL/6 mice (7 weeks old) were purchased from Japan SLC (Hamamatsu, Japan) and randomly assigned to the normal (n = 32) and diabetic groups (n = 33). Every 2 days, 2 to 4 mice from each group were sacrificed for histological analysis. Three normal control and 4 diabetic mice were kept alive until the wound completely healed for the quantification of wound closure. Mice in the diabetic group were fasted for 6 hours and then administered an intraperitoneal injection of freshly prepared streptozotocin (180 mg/kg body weight dissolved in citrate buffer at a pH of 4.5). Mice with blood glucose from the tail vein > 250 mg/dl were considered diabetic after one week of streptozotocin administration,[22] and these mice exhibited polydipsia, polyuria and weight loss. The experimental procedures were approved by the Institutional Review Committee of Juntendo University and conducted following the National Institutes of Health Guide for the Care and Use of Laboratory Animals.

The mice were anesthetized by 2.5% isoflurane inhalation. The dorsal skin was shaved, and 2 full-thickness wounds were created by a 6-mm-diameter biopsy punch under aseptic conditions. Each wound site was splinted using a metal ring attached to 5-0 silk sutures to prevent wound contraction. Either AMP-IBP5 (100 μM) or 0.01% acetic acid (vehicle) was topically applied after surgical excision every 2 days until the wounds were completely healed. The wounds were covered with a hydrocolloid dressing (Tegaderm; 3 M Health Care, Tokyo, Japan). Wound areas were digitally photographed and analyzed using ImageJ software

(National Institutes of Health, Bethesda, MD). The percentage of the wound area was calculated as follows: % wound area = (specific day area/initial wound area) × 100.

2.3 Histological, immunohistochemistry, immunofluorescence and vascular formation analysis

Formalin-fixed skin tissue from wound sites was embedded in paraffin. The wound tissue sections were stained with hematoxylin & eosin (H & E). The percentage of re-epithelialization was measured using the following formula: [original wound length (B) - distance between the newly re-epithelialization edges (A)]/B × 100. On day 4 postinjury, sections of wound tissue were fixed in 10% neutral buffered formalin, processed and embedded in paraffin. The sections were deparaffinized, hydrated, blocked with normal goat serum and then incubated with antibodies against Ki67, p-EGFR, p-STAT1 and p-STAT3 at 4°C overnight. After being dipped into biotin-conjugated goat anti-rabbit IgG for 1 hour, the slices were incubated with horseradish peroxidase-conjugated streptavidin for 30 minutes and then incubated with diaminobenzidine tetrahydrochloride solution. Sections were counterstained with hematoxylin and visualized using a light microscope. The sections were incubated with anti-CD31 antibody or IgG at 4°C overnight and incubated with the corresponding secondary antibody for 40 minutes. The sections were sealed with Vectashield antifade mounting medium containing DAPI and visualized under a laser scanning microscope 700 (Zeiss, Jena, Germany). A full-thickness skin specimen (1.5 cm × 1.8 cm) from the newly repaired skin at the wound site was

cut and washed 3 times with PBS. The skin specimen was placed upside down on a transparent Petri dish for cell/tissue culture and macroscopically visualized for subcutaneous vascular formation.

2.4 Total RNA extraction and real-time quantitative PCR

Total RNA was extracted from the skin tissue using the RNeasy Plus Universal Mini kit (Qiagen). cDNA was obtained using a ReverTra Ace qPCR RT kit (Toyobo, Osaka, Japan). Real-time PCR was performed with an Applied Biosystems StepOnePlus Real-time PCR system (Thermo Fisher Scientific, Waltham, MA) by using TaqMan Universal PCR Master Mix or SYBR Premix Ex Taq (Takara, Tokyo, Japan). TaqMan assay primers and probe mixes of the genes for murine *Ang* (Mm00833184_s1), *Egf* (Mm00438696_m1) and *Vegf* (Mm00437306_m1) were obtained from Applied Biosystems assays-on-demand. The data were normalized to β-actin or endogenous RPS18 expression ($2^{-\Delta\Delta CT}$ method). The primer information for SYBR Premix Ex Taq is shown in Supplementary Table 1.

2.5 Culture of primary human keratinocytes

Primary human epidermal keratinocytes from neonatal foreskin were purchased from Kurabo Industries (Osaka, Japan) and were cultured in HuMedia-KG2 (Kurabo Industries) as described previously.[23] Cells were maintained at 37°C and serially passaged at 60-70% confluence. The normal glucose concentration in the human epidermis is close to that in plasma (5.8 mM);[24] thus, we considered 6 mM to be normoglycemic. For hyperglycemic conditions,

cells were cultured in HuMedia containing 38 mM glucose for 48 hours as previously reported.[25] Mannitol was used as an osmotic control for high glucose (HG) treatment.

2.6 ELISA

Keratinocytes were cultured under normal conditions or 38 mM glucose for 48 hours and then incubated with 10 μM AMP-IBP5 for 48 hours. The amounts of ANG, EGF and VEGF in the cultured supernatants were measured with appropriate kits. In some experiments, keratinocytes were pretreated with various inhibitors for 2 hours before stimulation, and ELISA quantification was performed as described above.

2.7 Proliferation and migration assay

Keratinocyte proliferation was assessed using a 5-bromo-2'-deoxyuridine (BrdU) labeling and detection kit III (Roche Diagnostics, Indianapolis, IN) according to the manufacturer's protocol. Briefly, keratinocytes cultured in normal or HG conditions were trypsinized and seeded into 96-well plates (1×10^4 cells/well). Cells were stimulated with 5 μM AMP-IBP5 for 48 hours and incubated with 10 μM BrdU for 4 hours. The colorimetric reaction product was measured using a microplate reader at a wavelength of 450 nm.

Keratinocytes were seeded into collagen I-coated 96-well plates (0.5×10^5 cells/well) and cultured for 3 hours. Keratinocyte monolayers were scratched using a 96-well wound marker (Essen BioScience, Ann Arbor, MI). To exclude the influence of cell proliferation, 1 μg/ml mitomycin C (Fujifilm, Tokyo, Japan) was added for 2 hours before stimulation with 10 μM

AMP-IBP5 for 48 hours. Cells were stained with 0.5% crystal violet (Fujifilm, Tokyo, Japan). Images were recorded using a phase-contrast microscope (Keyence, Osaka, Japan). The wound area was measured with ImageJ software. Keratinocyte migration was also evaluated using a 48-well chemotaxis microchamber (Neuro Probe, Gaithersburg, MD). Keratinocytes (1.0×10^5 cells/well) were loaded into the upper chambers, which were separated from the lower chambers (5 μM AMP-IBP5) by a polyvinylpyrrolidone-free polycarbonate membrane with an 8-μm pore size (Neuro Probe). After a 6-hour incubation period, the membrane was stained with Diff-Quick (Kokusai Shiyaku, Kobe, Japan). The migrated cells were counted under a light microscope (Zeiss, Oberkochen, Germany).

2.8 Western blotting

Equal amounts of protein extracts were fractionated by 12.5% SDS–PAGE. After protein transfer, the polyvinylidene difluoride membranes (Millipore, Billerica, MA) were incubated with appropriate antibodies, developed with the Luminata Forte Western HRP substrate (Millipore, Billerica, MA) and visualized using Fujifilm LAS-4000 Plus (Fujifilm, Tokyo, Japan). Densitometric analysis was performed using ImageJ.

2.9 Statistical analysis

The statistical analysis was performed using either one-way ANOVA followed by the Dunnett's post hoc test for multiple groups or Student's *t* test for 2 groups (Prism 7, GraphPad Software, San Diego, CA). The results are presented as the means ± standard deviations. The

number of independent experiments carried out is indicated as *n*. $P < 0.05$ was considered significant.

3 Results

3.1 IGFBP5 was downregulated in diabetic mouse skin and in keratinocytes cultured in HG conditions

To evaluate whether AMP-IBP5 plays a role in diabetic wounds, we investigated the expression of IGFBP5, the parent protein of AMP-IBP5. The expression of *Igfbp5* was significantly decreased by 54.1% in the skin tissues of diabetic mice compared with those of normal control mice (Figure 1A). In addition, pretreatment of keratinocytes with 38 mM glucose for 48 hours to mimic diabetic conditions resulted in the downregulation of *IGFBP5* expression by 74.7% compared with that of the vehicle control (Figure 1B). Therefore, AMP-IBP5 might be reduced in the skin of diabetic subjects.

3.2 AMP-IBP5 promoted wound healing in diabetic mice

To determine the effect of AMP-IBP5 on *in vivo* wound healing, AMP-IBP5 or 0.01% acetic acid (vehicle) was topically applied to the wound area. AMP-IBP5-treated wounds exhibited accelerated wound closure compared with vehicle-treated controls in both normal and diabetic mice (Figure 2A). In control mice, AMP-IBP5-treated wounds started to significantly heal on day 4 and were completely healed at day 12, whereas in diabetic mice, the effect of AMP-IBP5 was first observed on day 8, and the wounds were completely healed at day 16 (Figure 2A, B).

Of note, we observed that spontaneous wound healing was complete on day 16 in normal mice, while in diabetic mice, this was observed on day 20 postinjury (data not shown). Histological comparison of wounds further confirmed delayed wound closure in diabetic mice and remarkable promotion of wound healing by AMP-IBP5 in both normal and diabetic mice (Figure 2C, D). This finding demonstrated that AMP-IBP5 effectively accelerated delayed wound healing in diabetic mice.

3.3 AMP-IBP5 rescued HG-induced impairments in angiogenesis

Impaired angiogenesis plays a critical role in the pathogenesis of diabetic wound healing.[26] We investigated the expression of angiogenic growth factors in wound tissues obtained at day 4 posttreatment. AMP-IBP5-treated wound tissues showed enhanced expression levels of *Ang*, *Egf* and *Vegf* (Figure 3A). Interestingly, in diabetic mice, vehicle-treated wounds exhibited markedly reduced expression levels of *Ang*, *Egf* and *Vegf*, and this attenuated expression was ameliorated in AMP-IBP5-treated wound tissues. The expression of other growth factors, such as fibroblast growth factor, transforming growth factor and platelet-derived growth factor, was not observed (data not shown).

The ability of AMP-IBP5 to rescue HG-induced angiogenesis impairment in diabetic mice was further confirmed by *in vitro* experiments. In keratinocytes cultured under normoglycemic conditions, AMP-IBP5 induced the production of ANG and VEGF, while an effect on EGF was not observed. The spontaneous secretion of ANG and VEGF was significantly reduced

under HG conditions, and the addition of AMP-IBP5 restored this secretion (Figure 3B). This finding suggests that AMP-IBP5 improves neovascularization in diabetic wounds.

Indeed, immunofluorescence staining of CD31, a marker of endothelial cells, showed that AMP-IBP5-treated wounds displayed increased numbers of CD31-positive blood vessels compared with vehicle-treated wounds in both normal and diabetic mice at day 4 postinjury (Figure 3C). Compared with wounds in normal mice, diabetic wounds showed decreased numbers of blood vessels in both the vehicle-treated and AMP-IBP5-treated groups. Similar data were observed by immunohistochemical staining with CD31 antibody (Figure S1). Furthermore, macroscopic observation of vessels in wounds also revealed that treatment with AMP-IBP5 increased the number of vessels in both normal and diabetic mice compared with vehicle treatment (Figure 3D). Collectively, AMP-IBP5 may promote neovascularization in diabetic subjects.

3.4 AMP-IBP5 attenuated HG-induced inhibition of keratinocyte proliferation and migration

Both keratinocyte proliferation and migration are indispensable in the wound repair process. The hyperglycemic milieu resulted in reduced cell proliferation (Figure 4A). The addition of AMP-IBP5 under both normoglycemic and hyperglycemic conditions markedly increased cell proliferation. Meanwhile, as shown in Figure 4B, increased proliferation was observed in the AMP-IBP5-treated wounds of normal and diabetic mice compared to that in vehicle-treated

wounds, as confirmed by Ki67-positive cells (Figure 4C). In addition, the inhibition of proliferation in the diabetic mouse wound area was rescued by AMP-IBP5 (Figure 4B, C).

Moreover, similar to the effects on cell proliferation, HG inhibited spontaneous cell migration, and this inhibition was as high as 40%. As expected, AMP-IBP5 not only increased keratinocyte migration under normal conditions but also rescued the HG-induced inhibition of cell migration (Figure 4D). Similarly, as demonstrated by the wound scratch assay, AMP-IBP5-treated wounds closed rapidly when cells were cultured under normoglycemic and hyperglycemic conditions compared with their respective controls (Figure 4E, F). Mannitol was used as an osmotic control and did not affect cell proliferation or migration.

3.5 AMP-IBP5 restored HG-induced keratinocyte dysfunction by activating the EGFR and STAT pathways

A previous study suggested that LL-37, which is involved in wound healing, induced keratinocyte migration via EGFR activation.[18] Furthermore, HG was reported to suppress EGFR signal activation in epithelial cells.[27] Thus, we hypothesized that AMP-IBP5 could activate the EGFR pathway, thereby resulting in the inhibition of HG-induced keratinocyte dysfunction. In keratinocytes cultured under normoglycemic conditions, stimulation with AMP-IBP5 for 15 minutes increased the phosphorylation of EGFR by nearly 2-fold compared with that of control cells (Figure 5A, left panel). Under hyperglycemic conditions, spontaneous

phosphorylation of EGFR decreased by nearly 30%; however, as expected, the addition of AMP-IBP5 markedly restored HG-induced EGFR inhibition.

STAT1 and STAT3 are two intracellular transcription factors that are known to be involved in the wound healing process.[28,29] Similar to the effect on EGFR, stimulation with AMP-IBP5 for 15 minutes or 2 hours induced the phosphorylation of STAT1 (Figure 5A, middle panel) and STAT3 (Figure 5A, right panel), respectively, under both normoglycemic and hyperglycemic conditions. We also observed that AMP-IBP5-treated normal wounds showed stronger expression of p-EGFR, p-STAT1 and p-STAT3 than vehicle-treated wounds, while diabetic wounds displayed weaker staining than normal wounds. Similar to the *in vitro* results, the treatment of diabetic wounds with AMP-IBP5 rescued the expression of p-EGFR, p-STAT1 and p-STAT3 (Figure 5B).

Furthermore, the AMP-IBP5-induced production of ANG and VEGF was significantly suppressed by AG1478 (EGFR inhibitor), fludarabine (STAT1 inhibitor) and cryptotanshinone (STAT3 inhibitor) (Figure 5C). Similarly, EGFR, STAT1 and STAT3 inhibitors markedly reduced AMP-IBP5-mediated proliferation (Figure 5D) and migration (Figure 5E, F) under HG conditions, suggesting crucial roles of the EGFR and STAT pathways in the AMP-IBP5-mediated restoration of keratinocyte functions in a hyperglycemic environment.

3.6 AMP-IBP5-mediated recovery of HG-induced keratinocyte dysfunction requires the activation of MAPK pathways

We previously reported that AMP-IBP5 promoted the phosphorylation of MAPKs, which are necessary for VEGF production by keratinocytes.[19] Moreover, recent studies demonstrated that HG-induced cell migration impairment was associated with JNK and p38 suppression.[24,30] Therefore, we examined the effect of AMP-IBP5 on MAPK activation in keratinocytes cultured in HG conditions. Spontaneous phosphorylation of ERK, JNK and p38 was significantly reduced in HG-treated cells; however, this inhibitory effect was largely abrogated by the addition of AMP-IBP5 (Figure 6A). Next, we confirmed that the MAPK pathways were necessary for AMP-IBP5-mediated activation of keratinocytes under HG conditions. U0126 (ERK inhibitor), JNK inhibitor II and SB203580 (p38 inhibitor) noticeably suppressed AMP-IBP5-induced VEGF production, whereas only U0126 and JNK inhibitor II suppressed ANG production (Figure 6B). Moreover, these MAPK inhibitors attenuated AMP-IBP5-induced keratinocyte proliferation (Figure 6C) and migration (Figure 6D, E), indicating that MAPKs are involved in the protective effect of AMP-IBP5 on keratinocytes under hyperglycemic conditions.

4 Discussion

Impaired diabetic wound healing is attributed to numerous risk factors, including hyperglycemia, hypoxia, inflammation, angiogenesis dysfunction and neuropathy.[9-12] Therefore, it is necessary to understand the complex pathogenesis of diabetic wound healing and develop holistic strategies to improve diabetic wound treatment. In this study, we

301 demonstrated that AMP-IBP5 significantly accelerated wound healing and ameliorated
302 impaired angiogenesis in diabetic mice. In the current study, we provide evidence that AMP-
303 IBP5 counteracts the deleterious effects of HG on keratinocytes, as demonstrated by *in vitro*
304 and *in vivo* experiments. The HG environment leads to inhibition of angiogenesis, proliferation
305 and activation of EGFR and STAT pathways, leading to delayed wound closure. Importantly,
306 AMP-IBP5 rescues HG-mediated impaired keratinocyte functions both *in vitro* and in a
307 diabetic mouse model.

308 Wound healing is a dynamic, complicated, and highly regulated biological process that is
309 supported by a myriad of cellular events. Prompt re-epithelialization and neovascularization
310 are essential in wound closure and tissue formation.[31] Evidence has shown that hyperglycemic
311 conditions reduce the expression of angiogenic factors, such as ANG and VEGF, in wound
312 tissue, decreasing the sprouting of new capillary angiogenesis.[26] Moreover, a topical gel
313 containing VEGF has been shown to accelerate wound closure in both mouse models and
314 patients with diabetic foot ulcers.[32,33] Herein, we revealed that AMP-IBP5 accelerated delayed
315 wound closure in diabetic mice. Moreover, AMP-IBP5 increased the expression of ANG and
316 VEGF both *in vivo* and *in vitro*. Intriguingly, AMP-IBP5 robustly rescued the impairment in
317 angiogenesis in diabetic mice and restored the levels of angiogenic factors in keratinocytes
318 cultured under hyperglycemic conditions, suggesting its crucial role in the induction of
319 neovascularization and wound closure.

Previous studies have demonstrated downregulated expression of AMPs in patients with diabetes, which explains why diabetic wounds show frequent bacterial infections that contribute to tissue destruction and delayed wound healing.[18,34] In this study, we also confirmed that the expression of IGFBP5, the parent protein of AMP-IBP5, was decreased under *in vivo* and *in vitro* diabetic conditions, suggesting that the absence of AMP-IBP5 could contribute to the impairment of diabetic wound healing.

Several AMPs activate the EGFR pathway to induce cell migration, which is an indispensable step in the wound healing process. Tokumaru et al. indicated that LL-37 induced keratinocyte migration via the transactivation of EGFR;[18] Grazia et al. suggested EGFR involvement in frog skin-derived AMP esculentin-1a (1-21) NH_2-induced migration of A549 cells.[35] In the current study, AMP-IBP5 not only activated EGFR but also rescued the attenuated activation of EGFR in keratinocytes cultured in HG conditions. However, further studies are needed to investigate how AMP-IBP5 activates EGFR.

STAT family proteins are intracellular transcription factors that act downstream of tyrosine kinase receptors, including EGFR, and play essential roles in cell proliferation, differentiation and angiogenesis.[36,37] Among the STAT family members, STAT3 is well known for its role in angiogenesis and wound healing.[37] In fact, STAT3 upregulates VEGF expression, thereby inducing angiogenesis, and the blockade of STAT3 signaling inhibits VEGF expression.[38] Furthermore, the levels of STAT1 are increased at wound sites after injury in a mouse model,[39]

339 and STAT3-deficient mice exhibit delayed skin wound healing.[40] Our observation that AMP-
340 IBP5 activates the STAT pathway is consistent with previous findings showing that AMPs
341 such as DRGN-1 and esculentin-1a (1-21) NH_2 enhanced keratinocyte migration through the
342 activation of STATs.[41] In addition, hBDs induce phosphorylation of STAT1 and STAT3, and
343 inhibition of these pathways attenuates hBD-mediated keratinocyte proliferation.[23] Here, the
344 production of ANG and VEGF was also mediated by STAT1 and STAT3, as indicated by the
345 inhibitory effects of specific inhibitors against STAT1 and STAT3. Interestingly, since ANG
346 acts as a high-affinity ligand for EGFR[42] and VEGF activates STAT1[43] and STAT3,[44] AMP-
347 IBP5-mediated effects on ANG and VEGF may in return participate in wound healing.

348 MAPK pathways are involved in keratinocyte activation induced by AMPs such as hBDs
349 and LL-37.[45] Herein, we demonstrated that ERK, JNK, and p38 levels were inhibited in
350 keratinocytes cultured in HG conditions; however, stimulation with AMP-IBP5 ameliorated
351 this inhibition. A previous study demonstrated that 72-hour HG (26 mM) treatment of
352 keratinocytes inhibited the phosphorylation of ERK.[46] Moreover, JNK phosphorylation in
353 fibroblasts decreased after culture in 30 mM glucose.[30] Li et al. suggested that p38 was
354 downregulated in keratinocytes maintained in a 36-hour HG environment (25 mM).[24] In
355 contrast, Lan et al. showed that phosphorylated ERK levels were increased in keratinocytes
356 stimulated with 26 mM glucose for 7 days.[47] This discrepancy in MAPK pathway activation
357 under hyperglycemic conditions might have been caused by different cell culture conditions,

358 such as the concentration of glucose and the duration of exposure to the HG environment. In
359 addition, subsequent to EGFR activation, MAPK pathways have been shown to act
360 downstream and engage in the wound healing process.[48] Therefore, the ability of AMP-IBP5
361 to activate the EGFR, STAT and MAPK pathways may explain the significant improvements
362 in diabetic wound healing.

363 In summary, AMP-IBP5 promoted keratinocyte proliferation and migration in an HG
364 environment and accelerated delayed angiogenesis and wound healing in diabetic mice. The
365 molecular mechanism of AMP-IBP5 involves the EGFR, STAT and MAPK pathways. The
366 potency of AMP-IBP5 might be due to its protective effect against glucotoxicity. We propose
367 that AMP-IBP5 might be a new therapeutic candidate for the treatment of diabetic wounds.

368 **Acknowledgments**: The authors wish to thank Michiyo Matsumoto for secretarial assistance
369 and the members of the Atopy (Allergy) Research Center for discussion.

370 **Funding**: This research was funded by a Grant-in-Aid for Scientific Research from the
371 Ministry of Education, Culture, Sports, Science and Technology, Japan (Grant number:
372 26461703 and 21K08309 to F.N.) and by the Atopy (Allergy) Research Center, Juntendo
373 University, Tokyo, Japan.

374 **Author Contributions**: Hainan Yue and François Niyonsaba designed the study, analyzed the
375 data, conducted the experiments, and wrote the manuscript. Pu Song, Nutda Sutthammikorn
376 and Yoshie Umehara contributed to the animal experiments. Juan Valentin Trujillo-Paez and

Hai Le Thanh Nguyen conducted the proliferation and migration experiments. Miho Takahashi, Ge Peng and Risa Ikutama performed cell culture and sample collection. Ko Okumura, Hideoki Ogawa, Shigaku Ikeda and François Niyonsaba contributed reagents and materials and coordinated the study.

Conflicts of Interest: The authors declare no conflicts of interest.

Abbreviations: **AMP**: antimicrobial peptide; **AMP-IBP5**: antimicrobial peptide derived from insulin-like growth factor-binding protein 5; **ANG**: angiogenin; **EGFR**: epidermal growth factor receptor; **ERK**: extracellular signal-regulated kinase; **hBD**: human β-defensin; HG: high glucose; **JNK**: c-Jun N-terminal kinase; **MAPK**: mitogen-activated protein kinase; **STAT**: signal transducer activator of transcription; **VEGF**: vascular endothelial growth factor.

References

1. Saeedi P, Petersohn I, Salpea P, et al. Global and regional diabetes prevalence estimates for 2019 and projections for 2030 and 2045: results from the international diabetes federation diabetes atlas. Diabetes Res Clin Pract. 2019;157(9):107843.

2. Zhang P, Lu J, Jing Y, et al. Global epidemiology of diabetic foot ulceration: a systematic review and meta-analysis. Ann Med. 2017;49(2):106-116.

3. Zhang Y, Lazzarini PA, McPhail SM, et al. Global disability burdens of diabetes-related lower-extremity complications in 1990 and 2016. Diabetes Care. 2020;43(5):964-974.

4. Liu S, He CZ, Cai YT, et al. Evaluation of negative-pressure wound therapy for patients

with diabetic foot ulcers: systematic review and meta-analysis. Ther Clin Risk Manag. 2017;13(4):533.

5. Frykberg RG, Banks J. Challenges in the treatment of chronic wounds. Adv wound care. 2015;4(9):560–582.

6. Jeffcoate WJ, Vileikyte L, Boyko EJ, et al. Current challenges and opportunities in the prevention and management of diabetic foot ulcers. Diabetes Care. 2018;41(4):645–652.

7. Spravchikov N, Sizyakov G, Gartsbein M, et al. Glucose effects on skin keratinocytes: implications for diabetes skin complications. Diabetes. 2001;50(7):1627–1635.

8. Hirsch T, Spielmann M, Zuhaili B, et al. Human beta-defensin-3 promotes wound healing in infected diabetic wounds. J Gene Med. 2009;11(3):220–228.

9. Botusan IR, Sunkari VG, et al. Stabilization of HIF-1alpha is critical to improve wound healing in diabetic mice. Proc Natl Acad Sci USA. 2008;105(49):19426–19431.

10. Theocharidis G, Veves A. Autonomic nerve dysfunction and impaired diabetic wound healing: the role of neuropeptides. Auton Neurosci. 2020;(223):102610.

11. Eming SA, Martin P, Tomic-Canic M. Wound repair and regeneration: mechanisms, signaling, and translation. Sci Transl Med. 2014;6(265):265sr6.

12. Pastar I, Stojadinovic O, et al. Epithelialization in wound healing: a comprehensive review. Advances in wound care. 2014;3(7):445–464.

13. Hu SC, Lan CE, High-glucose environment disturbs the physiologic functions of

415 keratinocytes: focusing on diabetic wound healing. J Dermatol Sci. 2016;84(2):121–127.

416 14. Baltzis D, Eleftheriadou I, Veves A. Pathogenesis and treatment of impaired wound
417 healing in diabetes mellitus: new insights. Adv Ther. 2014;31(8):817–836.

418 15. Osaki T, Sasaki K, Minamino N. Peptidomics-based discovery of an antimicrobial
419 peptide derived from insulin-like growth factor-binding protein 5. J Proteome Res.
420 2011;10(4):1870–1880.

421 16. Niyonsaba F, Nagaoka I, Ogawa H, et al. Multifunctional antimicrobial proteins and
422 peptides: natural activators of immune systems. Curr Pharm. Des. 2009;15(21):2393–
423 2413.

424 17. Lan CE, Wu CS, Huang SM, et al. High-glucose environment reduces human β-
425 defensin-2 expression in human keratinocytes: implications for poor diabetic wound
426 healing. Br J Dermatol. 2012;166(6):1221–1229.

427 18. Tokumaru S, Sayama K, Shirakata Y, et al. Induction of keratinocyte migration via
428 transactivation of the epidermal growth factor receptor by the antimicrobial peptide LL-
429 37. J Immunol. 2005;175(7):4662-4668.

430 19. Chieosilapatham P, Niyonsaba F, Kiatsurayanon C, et al. The antimicrobial peptide
431 derived from insulin-like growth factor-binding protein 5, AMP-IBP5, regulates
432 keratinocyte functions through Mas-related gene X receptors. J Dermatol Sci,
433 2017;88(1):117–125.

20. Chieosilapatham P, Yue H, Ikeda S, et al. Involvement of the lipoprotein receptor LRP1 in AMP-IBP5-mediated migration and proliferation of human keratinocytes and fibroblasts. J Dermatol Sci. 2020;99(3):158-167.

21. Niyonsaba F, Song P, Yue H, et al. Antimicrobial peptide derived from insulin-like growth factor-binding protein 5 activates mast cells via Mas-related G protein-coupled receptor X2. Allergy. 2020;75(1):203–207.

22. Deeds MC, Anderson JM, Armstrong AS, et al. Single dose streptozotocin-induced diabetes: considerations for study design in islet transplantation models. Lab Anim. 2011;45(3):131–140.

23. Niyonsaba F, Ushio H, Nakano N, et al. Antimicrobial peptides human β-defensins stimulate epidermal keratinocyte migration, proliferation and production of proinflammatory cytokines and chemokines. J Invest Dermatol. 2007;127(3):594–604.

24. Li L, Zhang J, Zhang Q, et al. High glucose suppresses keratinocyte migration through the inhibition of p38 MAPK/autophagy pathway. Front Physiol. 2019;10(24):1-13.

25. Okano J, Kojima H, Katagi M, et al. Hyperglycemia induces skin barrier dysfunctions with impairment of epidermal integrity in non-wounded skin of type 1 diabetic mice. PLoS One. 2016;11(11):e0166215.

26. Okonkwo UA, DiPietro LA. Diabetes and wound angiogenesis. Int J Mol Sci. 2017;18(7):14-19.

453 27. Xu KP, Li Y, Ljubimov AV, et al. High glucose suppresses epidermal growth factor
454 receptor/ phosphatidylinositol 3-kinase/akt signaling pathway and attenuates corneal
455 epithelial wound healing. Diabetes. 2009;58(5):1077-1085.
456 28. Beigel F, Friedrich M, Probst C, et al. Oncostatin M mediates STAT3-dependent
457 intestinal epithelial restitution via increased cell proliferation, decreased apoptosis and
458 upregulation of SERPIN family members. PLoS One. 2014;9(4):e93498.
459 29. Dai B, Cui M, Zhu M, et al. STAT1/3 and ERK1/2 synergistically regulate cardiac
460 fibrosis induced by high glucose. Cell Physiol Biochem. 2013;32(4):960-971.
461 30. Xuan YH, Huang BB, Tian HS, et al. High glucose inhibits human fibroblast cell
462 migration in wound healing via repression of bFGF-regulating JNK phosphorylation.
463 PLoS One. 2014;9(9):e108128.
464 31. Dreifke MB, Jayasuriya AA, Jayasuriya AG. Current wound healing procedures and
465 potential care. Mater Sci Eng C Mater Biol Appl. 2015;48(12):651-662.
466 32. Gomes A, Teixeira C, Ferraz R, et al. Wound-healing peptides for treatment of chronic
467 diabetic foot ulcers and other infected skin injuries. Molecules. 2017;22(10):1743.
468 33. Borena BM, Martens A, Broeckx SY, et al. Regenerative skin wound healing in
469 mammals: state-of-the-art on growth factor and stem cell based treatments. Cell Physiol
470 Biochem. 2015;36(1):1-23.
471 34. Rodríguez-Carlos A, Trujillo V, Gonzalez-Curiel I, et al. Host defense peptide RNase 7

is down-regulated in the skin of diabetic patients with or without chronic ulcers, and its expression is altered with metformin. Arch Med Res. 2020;51(4):327-335.

35. Di Grazia A, Cappiello F, Cohen H, et al. D-Amino acids incorporation in the frog skin-derived peptide esculentin-1a(1-21)NH2 is beneficial for its multiple functions. Amino Acids. 2015;47(12):2505-2519.

36. Jere SW, Abrahamse H, Houreld NN. The JAK/STAT signaling pathway and photobiomodulation in chronic wound healing. Cytokine Growth Factor Rev. 2017;38:73-79.

37. Chong HC, Chan JS, Goh CQ, et al. Angiopoietin-like 4 stimulates STAT3-mediated iNOS expression and enhances angiogenesis to accelerate wound healing in diabetic mice. Mol Ther. 2014;22(9):1593-1604.

38. Niu G, Wright KL, Huang M, et al. Constitutive Stat3 activity up-regulates VEGF expression and tumor angiogenesis. Oncogene. 2002;21(13):2000-2008.

39. Ishida Y, Kondo T, Takayasu T, et al. The essential involvement of cross-talk between IFN-gamma and TGF-beta in the skin wound-healing process. J Immunol. 2004;172(3):1848-1855.

40. Sano S, Takeda J, Yoshikawa K, et al. Tissue regeneration: hair follicle as a model. J Investig Dermatol Symp Proc. 2001;6(1):43-48.

41. Pfalzgraff A, Heinbockel L, Su Q, et al. Synthetic antimicrobial and LPS-neutralising

peptides suppress inflammatory and immune responses in skin cells and promote keratinocyte migration. Sci Rep. 2016;6:1-12.

42. Wang YN, Lee HH, Chou CK, et al. Angiogenin/Ribonuclease 5 is an EGFR ligand and a serum biomarker for erlotinib sensitivity in pancreatic cancer. Cancer Cell. 2018;33(4):752-769.

43. Bartoli M, Gu X, Tsai NT, et al. Vascular endothelial growth factor activates STAT proteins in aortic endothelial cells. J Biol Chem. 2000;275(43):33189-33192.

44. Bartoli M, Platt D, Lemtalsi T, et al. VEGF differentially activates STAT3 in microvascular endothelial cells. FASEB J. 2003;17(11):1562-1564.

45. Niyonsaba F, Ushio H, Nagaoka I, et al. The human beta-defensins (-1, -2, -3, -4) and cathelicidin LL-37 induce IL-18 secretion through p38 and ERK MAPK activation in primary human keratinocytes. J Immunol. 2005;175(3):1776-1784.

46. Song R, Ren L, Ma H, et al. Melatonin promotes diabetic wound healing in vitro by regulating keratinocyte activity. Am J Transl Res. 2016;8(11):4682-4693.

47. Lan CC, Wu CS, Huang SM, et al. High glucose environment enhanced oxidative stress and increased interleukin-8 secretion from keratinocytes. Diabetes. 2013;62(7):2530-2538.

48. Krall JA, Beyer EM, MacBeath G. High- and low-affinity epidermal growth factor receptor-ligand interactions activate distinct signaling pathways. PLoS One.

510 2011;6(1):e15945.

511

512 **Figure Legends**

513 **Figure 1 IGFBP5 expression was decreased in diabetic mouse skin and in high glucose-**
514 **induced keratinocytes**

515 (A) Biopsies were obtained from the dorsal skin of normal mice and streptozotocin-induced
516 diabetic mice. *Igfbp5* mRNA expression was evaluated by quantitative real-time quantitative
517 analysis using SYBR Premix Ex Taq. The results are shown as the mean ± SD. ### $P < 0.001$,
518 $n = 4$. (B) Human epidermal keratinocytes were cultured in normal (6 mM) and high glucose
519 (HG, 38 mM) conditions for 48 hours. *IGFBP5* mRNA expression was evaluated by
520 quantitative real-time quantitative analysis using SYBR Premix Ex Taq. The values represent
521 the mean ± SD. #### $P < 0.0001$, $n = 3$.

522 **Figure 2 AMP-IBP5 promoted wound healing in normal and diabetic mice**

523 Dorsal full-thickness dermal wounds were created on normal mice and streptozotocin-induced
524 diabetic mice and were treated with 0.01% acetic acid (vehicle) or 100 μM AMP-IBP5. (A)
525 Representative images of the wound area from day 0 to day 16 postinjury in normal mice and
526 diabetic mice. Scale bar = 1 mm. (B) The average wound area after different treatments was
527 calculated by ImageJ software. (C) Hematoxylin & eosin staining of wounds postinjury.
528 Arrows indicated wound edges. Scale bar = 0.2 mm. (D) Quantitative analysis of the percentage
529 of re-epithelialization postinjury. The values represent the mean ± SD. * $P < 0.05$, ** $P < 0.01$,
530 **** $P < 0.0001$ for comparisons between vehicle-treated wounds and AMP-IBP5-treated

wounds in normal mice. # $P < 0.05$, ## $P < 0.01$, ### $P < 0.001$ for comparisons between vehicle-treated wounds in normal mice and those in diabetic mice. & $P < 0.05$, && $P < 0.01$ for comparisons between vehicle-treated wounds and AMP-IBP5-treated wounds in diabetic mice, $n = 3$ wound areas/group.

Figure 3 AMP-IBP5 rescued high glucose-induced impaired angiogenesis in diabetic mice

(A) The mRNA expression of *Ang*, *Egf*, *Vegf* in wounded skin from normal mice and diabetic mice treated with 0.01% acetic acid (vehicle) or 100 μM AMP-IBP5 at day 4 postinjury. (B) Keratinocytes were cultured in 6 mM normal medium (NM) or 38 mM high glucose medium (HGM) for 48 hours and stimulated with 10 μM AMP-IBP5 for 48 hours. Mannitol (38 mM) was used as an osmotic control. The levels of ANG, EGF and VEGF were measured by ELISA. (C) Representative images of wounds from normal and diabetic mice treated with 0.01% acetic acid (vehicle) and 100 μM AMP-IBP5. On day 4 postinjury, sections were stained with immunofluorescent anti-CD31 antibody, and CD31-positive staining is indicated by yellow arrows; scale bar = 50 μm. (D) Representative images of the macroscopic appearance of blood vessels at the wound sites on day 4, day 8, day 12, and day 16 postinjury in normal mice and diabetic mice treated with 0.01% acetic acid (vehicle) and 100 μM AMP-IBP5. Scale bar = 1 mm. ** $P < 0.01$, *** $P < 0.001$, **** $P < 0.0001$ for comparisons between vehicle and AMP-IBP5 in normal mice or normal medium (NM). # $P < 0.05$, ## $P < 0.01$, ### $P < 0.001$ for

comparisons between vehicle treatment in normal mice or normal medium (NM) and diabetic mice or high glucose medium (HGM). & $P < 0.05$, && $P < 0.01$, &&& $P < 0.001$ for comparisons between vehicle and AMP-IBP5 in diabetic conditions, $n = 3$.

Figure 4 AMP-IBP5 attenuated high glucose-induced inhibition of keratinocyte proliferation and migration

Keratinocytes cultured in normal medium (NM), high glucose medium (HGM) or mannitol-containing medium for 48 hours were trypsinized and used for different assays. (A) Cells were stimulated with 5 μM AMP-IBP5 in normal medium (NM) or high glucose medium (HGM) for 48 hours, and cell proliferation was assessed. (B) Immunohistochemical staining of Ki67 in the wounds 4 days after treatment. Scale bar = 200 μm. (C) The number of Ki67-positive cells was counted in 3 high-power fields of wound sections. (D) Keratinocytes in the upper wells of the microchamber were allowed to migrate for 6 hours toward vehicle or 5 μM AMP-IBP5 in normal medium (NM) or high glucose medium (HGM). Migrated cells were counted in 3 high-power fields (HPFs) under a light microscope. (E) Keratinocytes were treated with 1 μg/ml mitomycin C for 2 hours. A scratch assay was performed. After treatment with mannitol or 10 μM AMP-IBP5 in normal medium (NM) or high glucose medium (HGM) for 48 hours, keratinocytes were stained with crystal violet, and images were recorded, scale bar = 200 μm. (F) The average wound areas were calculated using ImageJ software. The results are shown as the mean ± SD. * $P < 0.05$, ** $P < 0.01$, *** $P < 0.001$ for comparisons between vehicle and

AMP-IBP5 in normal mice or normal medium (NM). # $P < 0.05$, ## $P < 0.01$, ### $P < 0.001$ for comparisons between vehicle treatment in normal mice or normal medium (NM) and diabetic mice or high glucose medium (HGM). & $P < 0.05$, && $P < 0.01$, &&& $P < 0.001$ for comparisons between vehicle and AMP-IBP5 in diabetic conditions, n = 3-4.

Figure 5 AMP-IBP5 restored high glucose-induced keratinocyte dysfunction by activating the EGFR and STAT pathways

(A) Keratinocytes were cultured in normal, high glucose or mannitol-containing medium for 48 hours, stimulated with 10 μM AMP-IBP5 for 15 minutes for EGFR and STAT1 and 2 hours for STAT3, and then subjected to Western blotting using antibodies against phosphorylated or unphosphorylated EGFR, STAT1 or STAT3. Bands were quantified using densitometry. The results are expressed as the mean ± SD. *** $P < 0.001$, **** $P < 0.0001$ for comparisons between nonstimulated and AMP-IBP5-stimulated cells in normal medium. # $P < 0.05$, ## $P < 0.01$ for comparisons between nonstimulated cells in normal medium and high glucose medium (HGM). & $P < 0.05$, && $P < 0.01$, &&&& $P < 0.0001$ for comparisons between nonstimulated cells and AMP-IBP5-stimulated cells in high glucose medium, n = 3. (B) Immunohistochemistry staining of wound sections 4 days postinjury. (C), (D) and (E) Keratinocytes cultured under high glucose (38 mM) conditions were pretreated with 0.1% DMSO (vehicle), 50 nM AG1478, 100 μM fludarabine and 2.5 μg/mL cryptotanshinone (CT) for 2 hours and exposed to 10 μM AMP-IBP5 for 48 hours. (C) The levels of ANG and VEGF

588 in culture supernatants were measured by ELISA. (D) Keratinocyte proliferation was assessed
589 using the BrdU labeling detection kit. (E) Keratinocyte migration was analyzed by scratch
590 wound assays *in vitro*; scale bar = 200 μm. (F) The average wound areas were calculated using
591 ImageJ software. The results are expressed as the mean ± SD. * $P < 0.05$, ** $P < 0.01$, **** P
592 < 0.0001 for comparisons between vehicle and AMP-IBP5. # $P < 0.05$, ## $P < 0.01$, ### $P <$
593 0.001, #### $P < 0.0001$ for comparisons between AMP-IBP5-treated cells with or without
594 inhibitors, $n = 3$.

595 **Figure 6 AMP-IBP5-mediated amelioration of high glucose-induced keratinocyte**
596 **dysfunction requires the activation of MAPK pathways**

597 (A) Keratinocytes were cultured in normal, high glucose or mannitol-containing medium for
598 48 hours, stimulated with 10 μM AMP-IBP5 for 15 minutes for JNK, 30 minutes for ERK and
599 60 minutes for p38, and then subjected to Western blotting using antibodies against
600 phosphorylated or unphosphorylated ERK, JNK and p38. Bands were quantified using
601 densitometry. The results are shown as the mean ± SD. * $P < 0.05$, *** $P < 0.001$, **** $P <$
602 0.0001 for comparisons between nonstimulated and AMP-IBP5-stimulated cells in normal
603 medium. # $P < 0.05$ for comparisons between nonstimulated cells in normal medium and high
604 glucose medium (HG). && $P < 0.01$, &&& $P < 0.001$ for comparisons between nonstimulated
605 cells and AMP-IBP5-stimulated cells in high glucose medium, $n = 3$. (B), (C) and (D)
606 Keratinocytes incubated with 38 mM glucose were pretreated with 0.1% DMSO (vehicle), 10

μM U0126, 10 μM SB203580 and 10 μM JNK inhibitor II (JNK inh II) for 2 hours and exposed to 10 μM AMP-IBP5 for 48 hours. (B) The levels of ANG and VEGF in culture supernatants were measured by ELISA. (C) Keratinocyte proliferation was assessed using the BrdU labeling detection kit. (D) Keratinocyte migration was analyzed by scratch wound assay *in vitro*, scale bar = 200 μm. (E) The average wound areas were calculated using ImageJ software. The results are expressed as the mean ± SD. ** $P < 0.01$, **** $P < 0.0001$ for comparisons between vehicle and AMP-IBP5. # $P < 0.05$, ## $P < 0.01$, #### $P < 0.0001$ for comparisons between AMP-IBP5-treated cells with or without inhibitors, $n = 3$.

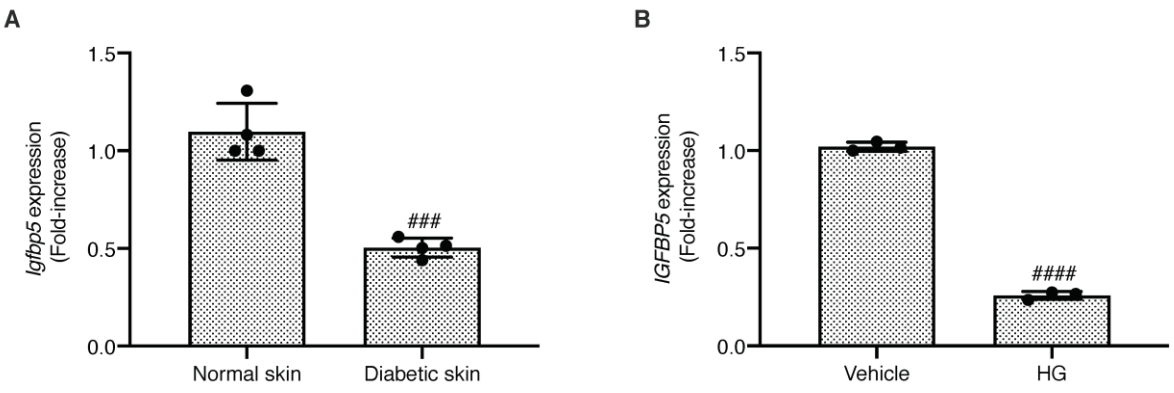
A
1.5
1.0
0.5
0.0
Igfbp5 expression
(Fold-increase)
###
Normal skin
Diabetic skin
B
1.5
1.0
0.5
0.0
IGFBP5 expression
(Fold-increase)
####
Vehicle
HG

Figure 1

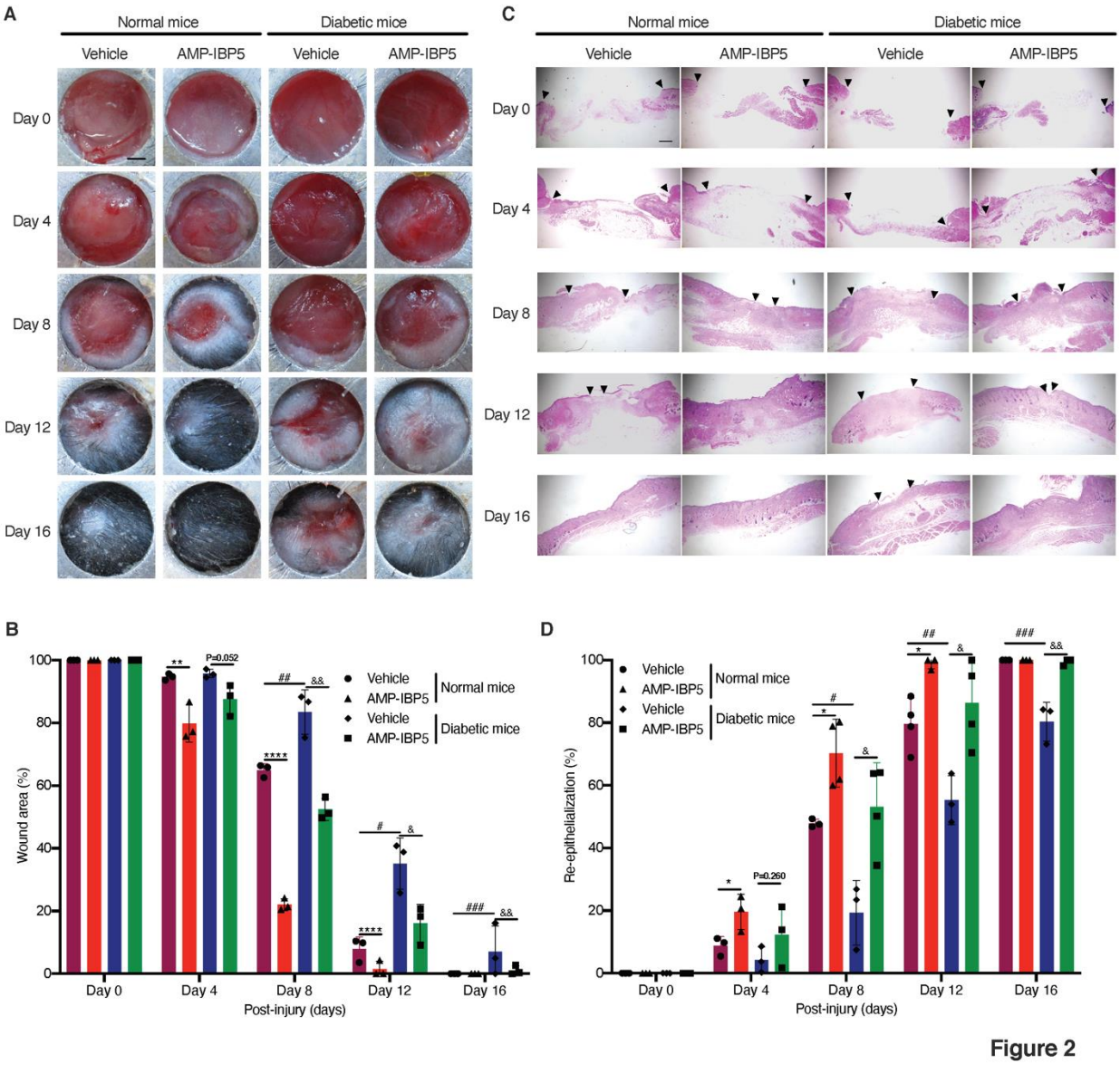
A
Normal mice
Diabetic mice
Vehicle
AMP-IBP5
Vehicle
AMP-IBP5
Day 0
Day 4
Day 8
Day 12
Day 16
C
Normal mice
Diabetic mice
Vehicle
AMP-IBP5
Vehicle
AMP-IBP5
Day 0
Day 4
Day 8
Day 12
Day 16
B
Wound area (%)
100
80
60
40
20
0
**
P=0.052
##
&&
****
#
&
****
###
&&
Vehicle
AMP-IBP5
Normal mice
Vehicle
AMP-IBP5
Diabetic mice
Day 0
Day 4
Day 8
Day 12
Day 16
Post-injury (days)
D
Re-epithelialization (%)
100
80
60
40
20
0
Vehicle
AMP-IBP5
Normal mice
Vehicle
AMP-IBP5
Diabetic mice
*
P=0.260
#
*
&
##
*
&
###
&&
Day 0
Day 4
Day 8
Day 12
Day 16
Post-injury (days)

Figure 2

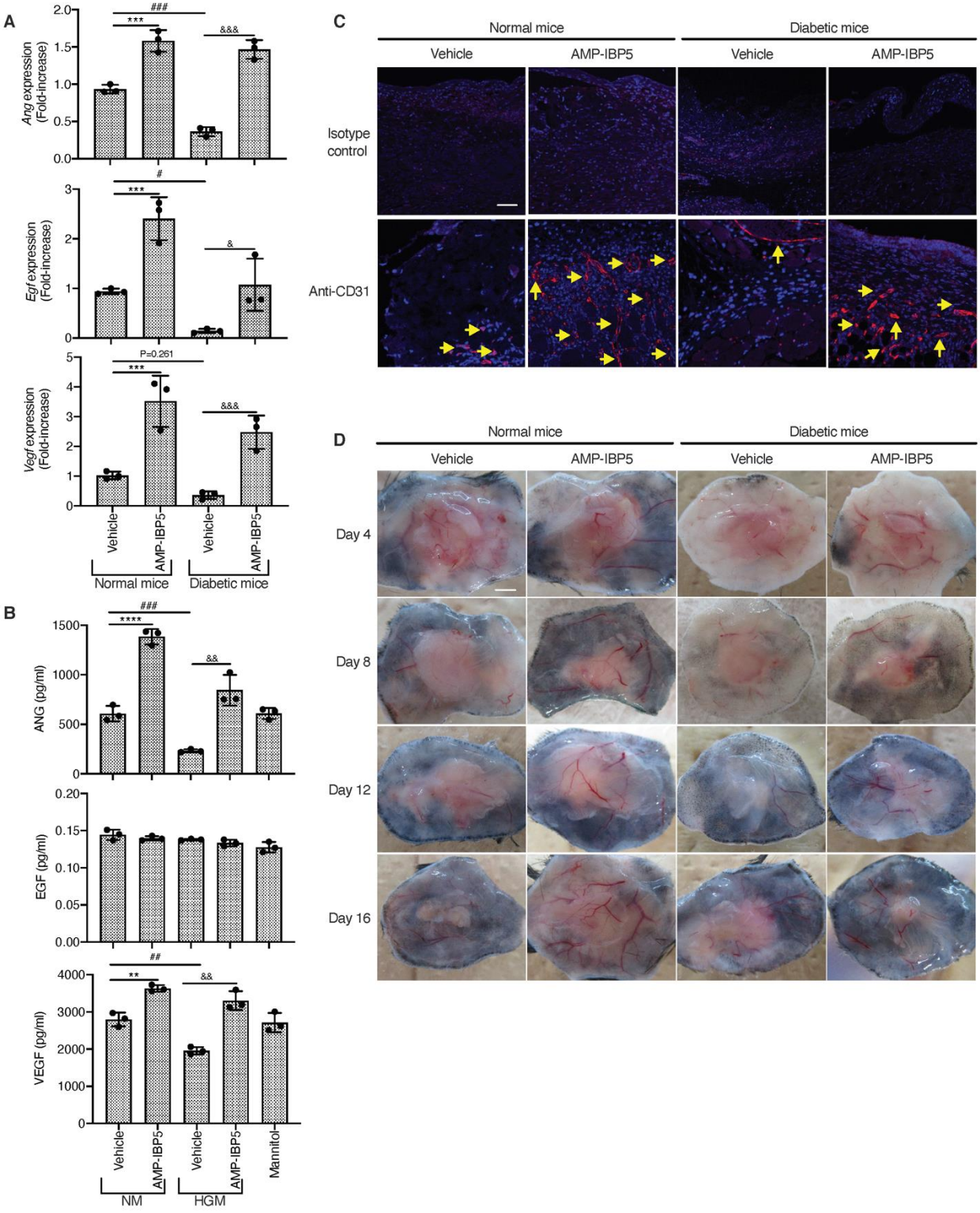
A
Ang expression (Fold-increase)
Egf expression (Fold-increase)
Vegf expression (Fold-increase)
P=0.261
Vehicle
AMP-IBP5
Normal mice
Diabetic mice
B
ANG (pg/ml)
EGF (pg/ml)
VEGF (pg/ml)
Vehicle
AMP-IBP5
Mannitol
NM
HGM
C
Normal mice
Diabetic mice
Vehicle
AMP-IBP5
Isotype control
Anti-CD31
D
Normal mice
Diabetic mice
Vehicle
AMP-IBP5
Day 4
Day 8
Day 12
Day 16

Figure 3

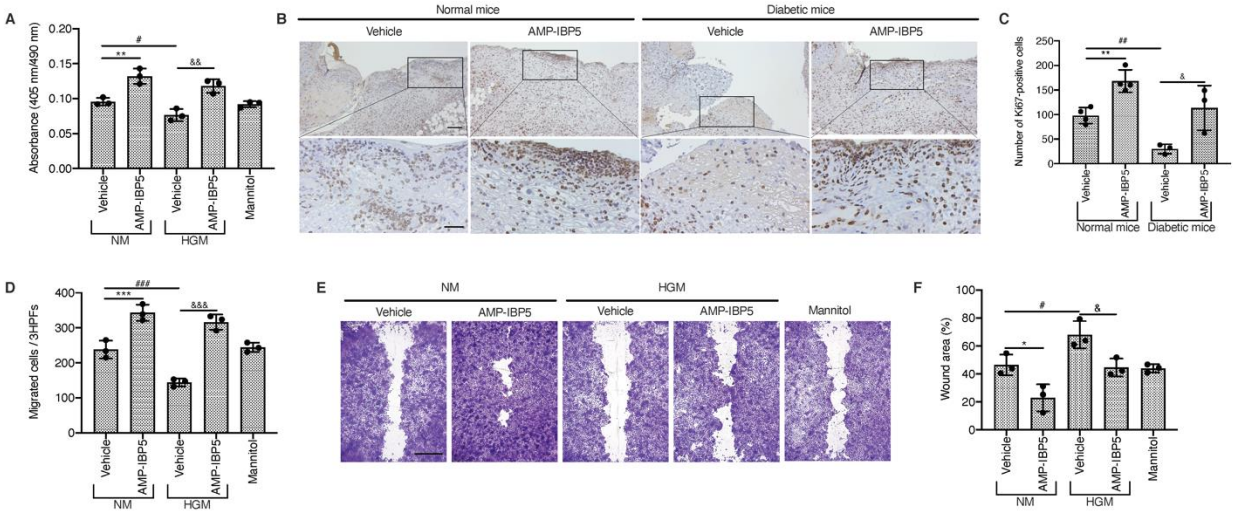
A
Absorbance (405 nm/490 nm)
0.20
0.15
0.10
0.05
0.00
#
**
&&
Vehicle
AMP-IBP5
Vehicle
AMP-IBP5
Mannitol
NM
HGM
B
Normal mice
Diabetic mice
Vehicle
AMP-IBP5
Vehicle
AMP-IBP5
C
Number of Ki67-positive cells
250
200
150
100
50
0
##
**
&
Vehicle
AMP-IBP5
Vehicle
AMP-IBP5
Normal mice
Diabetic mice
D
Migrated cells / 3HPFs
400
300
200
100
0
###
***
&&&
Vehicle
AMP-IBP5
Vehicle
AMP-IBP5
Mannitol
NM
HGM
E
NM
HGM
Vehicle
AMP-IBP5
Vehicle
AMP-IBP5
Mannitol
F
Wound area (%)
100
80
60
40
20
0
#
&
*
Vehicle
AMP-IBP5
Vehicle
AMP-IBP5
Mannitol
NM
HGM

Figure 4

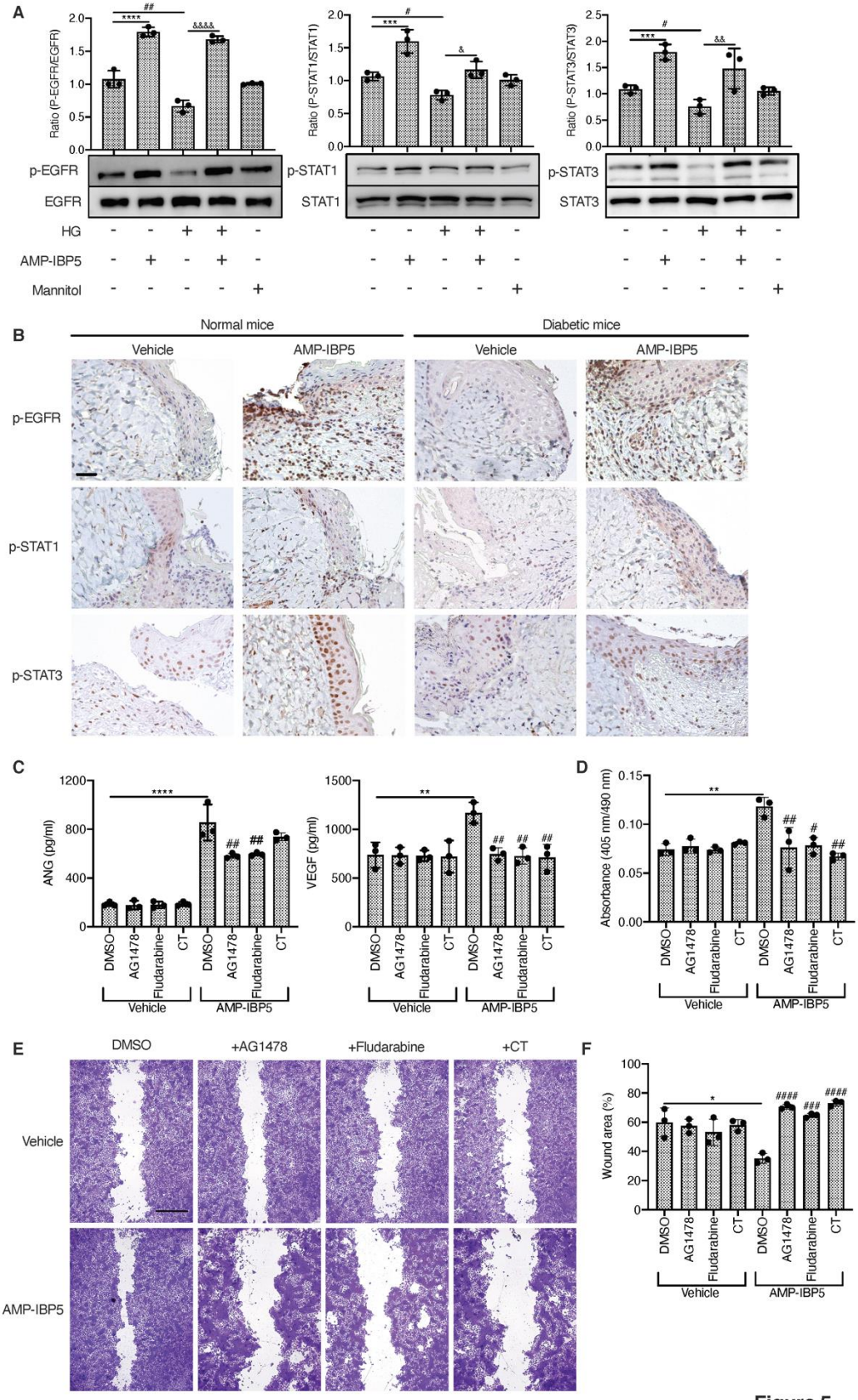
A
Ratio (P-EGFR/EGFR)
Ratio (P-STAT1/STAT1)
Ratio (P-STAT3/STAT3)
p-EGFR
EGFR
p-STAT1
STAT1
p-STAT3
STAT3
HG
AMP-IBP5
Mannitol
B
Normal mice
Diabetic mice
Vehicle
AMP-IBP5
p-EGFR
p-STAT1
p-STAT3
C
ANG (pg/ml)
VEGF (pg/ml)
DMSO
AG1478
Fludarabine
CT
Vehicle
AMP-IBP5
D
Absorbance (405 nm/490 nm)
E
DMSO
+AG1478
+Fludarabine
+CT
Vehicle
AMP-IBP5
F
Wound area (%)

Figure 5

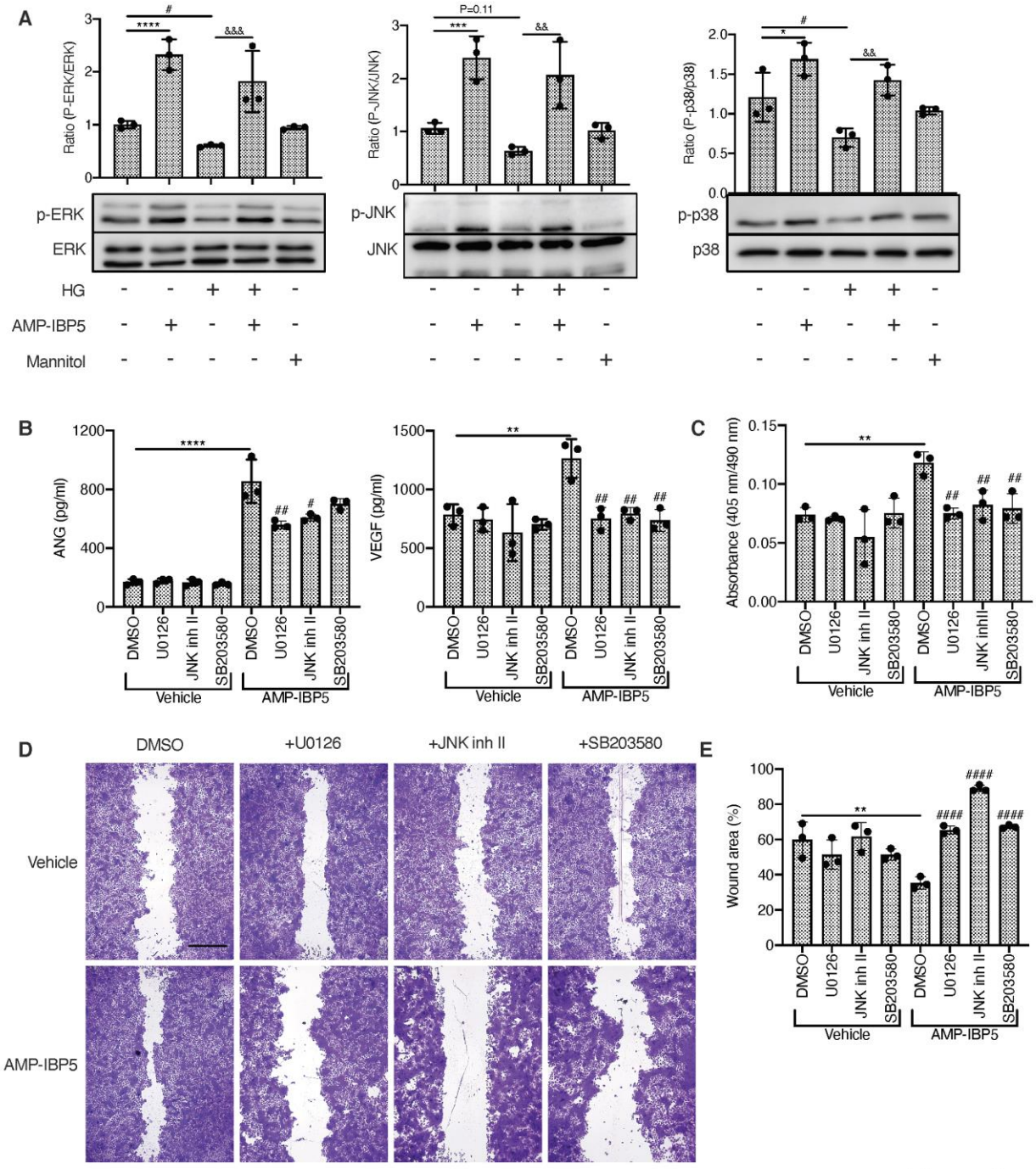
A
Ratio (P-ERK/ERK)
p-ERK
ERK
Ratio (P-JNK/JNK)
p-JNK
JNK
Ratio (P-p38/p38)
p-p38
p38
P=0.11
HG
AMP-IBP5
Mannitol
B
ANG (pg/ml)
VEGF (pg/ml)
DMSO
U0126
JNK inh II
SB203580
Vehicle
AMP-IBP5
C
Absorbance (405 nm/490 nm)
JNK inhII
D
DMSO
+U0126
+JNK inh II
+SB203580
Vehicle
AMP-IBP5
E
Wound area (%)

Figure 6